www.elsevier.com/locate/jcrysgro

Growth and characterization of epitaxial Ti_3GeC_2 thin films on 4 H-SiC(0 0 0 1)

K. Buchholt, P. Eklund, J. Jensen, J. Lu, R. Ghandi, M. Domeij, C.M. Zetterling, G. Behan, H. Zhang, A. Lloyd Spetz, L. Hultman

PII: S0022-0248(12)00068-1
DOI: doi:10.1016/j.jcrysgro.2012.01.020
Reference: CRYS20606

To appear in: *Journal of Crystal Growth*

Received date: 28 October 2011
Revised date: 11 January 2012
Accepted date: 14 January 2012

Cite this article as: K. Buchholt, P. Eklund, J. Jensen, J. Lu, R. Ghandi, M. Domeij, C.M. Zetterling, G. Behan, H. Zhang, A. Lloyd Spetz and L. Hultman, Growth and characterization of epitaxial Ti_3GeC_2 thin films on 4 H-SiC(0 0 0 1), *Journal of Crystal Growth,* doi:10.1016/j.jcrysgro.2012.01.020

Growth and characterization of epitaxial Ti_3GeC_2 thin films on 4H-SiC(0001)

K. Buchholt[a], P. Eklund[a], J. Jensen[a], J. Lu[a], R. Ghandi[b], M. Domeij[b],

C. M. Zetterling[b], G. Behan[c], H. Zhang[c], A. Lloyd Spetz[a], and

L. Hultman[a]

[a] *Department of Physics, Chemistry and Biology (IFM), Linköping University, SE-581 83 Linköping, Sweden*

[b] *School of Information and Communication Technology, KTH, Royal Institute of Technology, Electrum 229, SE-164 40 Kista-Stockholm, Sweden*

[c]*School of Physics and Centre for Research on Adaptive Nanostructures and Nanodevices (CRANN), Trinity College Dublin, Dublin 2, Republic of Ireland*

* Corresponding author. E-mail: kribu@ifm.liu.se

Abstract Epitaxial Ti_3GeC_2 thin films were deposited on 4° off-cut 4H-SiC(0001) using magnetron sputtering from high purity Ti, C, and Ge targets. Scanning electron microscopy and helium ion microscopy show that the Ti_3GeC_2 films grow by lateral step-flow with {11 0} faceting on the SiC surface. Using elastic recoil detection analysis, atomic force microscopy, and X-Ray diffraction the films were found to be substoichiometric in Ge with the presence of small Ge particles at the surface of the film.

Keywords A1. Surface structure, A1. Atomic force microscopy, A1. Helium ion microscopy, A3. Physical vapor deposition processes, B1. Titanium compound

1 Introduction

The group of inherently nanolaminated ternary carbides and nitrides called MAX phases exhibits a unique combination of metallic and ceramic properties, and has attracted considerable interest since the 1990s when Barsoum et al. reported on the fabrication and characterization of Ti_3SiC_2 [1], and shortly thereafter Ti_3GeC_2 [2]. The MAX phases have the general chemical formula $M_{n+1}AX_n$ where n=1, 2, or 3, and *M* is an early transition element, *A* is an A-group element, and *X* is C or N. For reviews on the topic, see references [3- 5].

Ti_3SiC_2 is known to form after high temperature annealing of Ti-, and Ti/Al-based contacts on SiC [6-10]. In recent publications, we have reported on the ohmic contact properties of sputter-deposited Ti_3SiC_2 on 4H-SiC(0001), and investigated the step-flow growth mode of epitaxially grown Ti_3SiC_2 layers on SiC [11, 12].

Ti-A-C MAX phase material systems related through their A-group elements from group 14 include Ti-Si-C, Ti-Ge-C, Ti-Sn-C, and Ti-Pb-C. These material systems display differences in phase distribution. The Ti-Si-C system contains the phases Ti_3SiC_2 and Ti_4SiC_3, where the former is the most studied member of the MAX phase family. In the Ti-Ge-C system, the 211, 312, and 413 phases Ti_2GeC, Ti_3GeC_2, and Ti_4GeC_3 have been epitaxially grown in thin-film form onto Al_2O_3(0001) substrates using magnetron sputtering. Four-point probe measurements of the epitaxial Ti-Ge-C thin films show them to be good conductors, with conductivity values for Ti_3GeC_2 films comparable to those of Ti_3SiC_2 films [13]. Studies on the electronic transport properties of MAX phases using the model system Ti_2GeC showed isotropic electronic transport behavior [14]. The Ti-Sn-C system

contains the two phases Ti_2SnC and Ti_3SnC_2 while in the Ti-Pb-C system the only known phase is Ti_2PbC. Resistivity values for magnetron sputtered Ti_2SnC thin films have been reported to be three times higher than for Ti_2GeC films, however, the crystalline quality was lower for the Ti_2SnC films [15]. Resistivity values for Ti_2PbC are not available in literature due to difficulty in fabricating samples pure enough for characterization [16], and the material has not been synthesized in thin film form.

Studies of M_2AlC (M = Ti, V, Cr) show that substitutions at the M-site leads to an increase in resistivity [17]. The same trend can be observed for M_2GeC (M = Ti, V, Cr) where the highest resistivity is reported for Cr_2GeC films [15, 18, 19]. In the M-Ge-C system, the influence of M-site solid solutions on material properties has been studied for $(Ti,V)_{n+1}GeC_n$ [20] and $(Cr_{1-x}V_x)_2GeC$ [21] thin films.

The good conductivity values reported for Ti-Ge-C thin films make the material system interesting to study as a candidate for ohmic contact layer on SiC. Investigating Ti_3GeC_2 provides an opportunity to study the influence of substituting Si (used in our previous studies of Ti_3SiC_2) with Ge in a 312 Ti-A-C MAX phase.

Although Ti_3SiC_2 and Ti_3GeC_2 are isostructural phases with similar properties, they exhibit differences in thermal and mechanical properties [22] and the growth behavior of sputtered Ti_3GeC_2 thin films on 4H-SiC is not known; nor are its electrical contact properties. Here, we investigate the epitaxial growth of Ti_3GeC_2 thin films on 4° off-cut 4H-SiC(0001) substrates using DC magnetron sputtering from three sources. We present results on a layer-by-layer growth mode of Ti_3GeC_2 on the stepped surface of SiC and discuss the similarities and differences to the related phase Ti_3SiC_2.

2 Experimental details

A 4H-SiC *n*-type wafer, Si-face, with a 4° off-cut, from SiCrystal [23] was used as substrate. The wafer has a 1 μm thick *p*- (4×10^{15} cm^{-3}) doped epitaxially grown SiC layer with a 0.8 μm *n*- (1.5×10^{19} cm^{-3}) doped epitaxially grown SiC layer on top. The doping atoms used for the epilayers were Al and N for the *p*- and *n*-type, respectively, and were grown at the Institute Acreo [24]. Prior to deposition the substrates were ultrasonically cleaned in acetone and isopropanol for 5 minutes each. The substrates were then blown dry in N_2 gas and immediately loaded into the ultra-high vacuum sputtering system. The substrates were heated to the deposition temperature of 800 °C and left to stabilize at that temperature for 1 h prior to deposition. Immediately before deposition the substrates were plasma etched for 30 minutes through operating the Ti-target at 25 mA in high purity Ar discharges, while applying a negative bias of -50 V to the substrate, in order to remove any remaining surface oxide on the SiC substrate [12].

Ti_3GeC_2 films were grown by DC magnetron sputtering, using high purity C, Ge, and Ti targets, using an experimental setup described elsewhere [25]. All depositions were performed at a constant pressure of ~0.5 Pa in high purity Ar discharges. The magnetrons were operated in current-regulation mode, with the target currents fixed at 310 mA for Ti, 370 mA for C, and 80 mA for the Ge target. The duration of the deposition was 1 h, resulting in approximately 200 nm thick films.

The as-deposited films were characterized by θ-2θ X-ray diffraction (XRD) measurements, performed in a Philips PW 1820 diffractometer with Cu Kα radiation, operated at 40 kV and 40 mA. Alignment of the instrument using the (0004) SiC substrate peak gives an offset of ~4° due to the 4° off-cut of the SiC substrate.

Surface morphology was investigated using secondary-electron images from a Leo 1550 Gemini scanning electron microscope (SEM), using a 5 kV accelerating voltage, and helium ion microscopy (HIM), using an ORION PLUS microscope from Carl Zeiss SMT. Plan-view images were obtained using 30 keV He^+ ions. The imaging was performed by detecting secondary electrons, using an Everhart-Thornley detector. Prior to observation the sample was plasma cleaned to remove hydrocarbons contamination on the sample surface. A Dimension 3100 atomic force microscopy (AFM), was also used to investigate surface morphology. Cross-sectional samples for transmission electron microscopy (TEM) using a Tecnai G2 TF20UT FEG, were prepared by gluing two pieces of thin film samples face to face and clamping them with a Ti grid. The sandwich-like specimen was polished to a thickness of about 50 μm using diamond grinding papers and thereafter ion milled to electron transparency using a Gatan PIPS instrument at 5 and 2 kV accelerating voltage.

Elemental depth profiles of the as-deposited films were performed using time-of-flight elastic recoil detection analysis (ToF-ERDA). Here, a 40 MeV $^{127}I^{9+}$ beam was directed to the films at an incident angle of 67.5° with respect to the surface normal, and the recoils were detected at an angle of 45° [26, 27]. All spectra were analyzed using the CONTES code [28], where the recoil energy of each element was converted to relative atomic concentration profiles.

Mesa etching for isolation of the highly doped epitaxial top SiC layer and definition of the contact pads for the linear transmission line model measurements (TLM) was performed using a two-step inductively coupled plasma (ICP) dry etching system with a 1 μm thick silicon dioxide etching mask. The TLM structures consists of six contact pads (100 μm wide) separated by 5, 10, 15, 20, and 25 μm. Current-

voltage (I-V) measurements were performed in air at room temperature, using a two-probe station connected to a KEITHLEY 4200-SCS Semiconductor Characterization System.

3 Results and discussion

Figure 1 shows a XRD pattern from a typical Ti-Ge-C film. Except for peaks from the SiC substrate, the Ti-Ge-C film displays only *000ℓ* Ti_3GeC_2 reflections, consistent with peak positions reported for epitaxially grown Ti_3GeC_2 on Al_2O_3(0001) substrates [13, 29]. The presence of TiC in the samples cannot be excluded using XRD since the SiC(0004) substrate peak overlaps with the TiC(111) peak (ICDD PDF 22-1317 and 32-1383 for SiC and TiC, respectively). In fact, TEM showed that trace amounts of TiC inclusions are present. The presence of only *000ℓ* diffraction peaks shows that the Ti_3GeC_2 films are *000ℓ*-oriented on the 4H-SiC(0001) substrate with a 4° angle relative to the substrate surface, following the substrate off-cut angle. This corresponds to the growth mode for Ti_3SiC_2 on similar off-cut 4H-SiC(0001) wafers [12]. The lattice parameters for Ti_3GeC_2 are a=3.077 Å and c=17.76 Å (ICDD PDF 20-0451). These values are very similar to the values for Ti_3SiC_2, where a=3.062 Å and c=17.637 Å (ICDD PDF 40-1132). This means that Ti_3GeC_2, just like Ti_3SiC_2, has a very small lattice mismatch, less than 0.2%, of the basal planes with 4H-SiC, where a=3.073 Å and c=10.053 Å (ICDD PDF 22-1317).

In Figure 2(a), a low magnification TEM image shows both the SiC substrate and the epitaxial Ti_3GeC_2 film grown on top. It can be seen that the Ti_3GeC_2 film growth follows the 4° off-cut orientation of the SiC substrate surface, which is consistent with the XRD observations. Figure 2(b) shows a high-resolution image of the film, which consists predominantly of Ti_3GeC_2. Only trace amounts of TiC(111) inclusions in the Ti_3GeC_2 films were observed.

Figure 3 is a ToF-ERDA depth profile of a Ti_3GeC_2 sample and shows the composition to be 51 at. % Ti, 13 at. % Ge, and 36 at. % C with a margin of error of less than 2 at. %. Oxygen is only observed at the surface of the Ti_3GeC_2 films; no oxygen is found throughout the films or at the interface between the Ti_3GeC_2 and the SiC (below the detection limit). This is to be expected since a plasma-etching step was performed prior to deposition, in order to remove surface oxide on the SiC substrate [11].

The composition obtained from the ToF-ERDA depth profile deviates from a stoichiometric Ti_3GeC_2 composition. Since our films are virtually phase pure (neglecting the trace amounts of TiC_x), we conclude that our films are substoichiometric in Ge with $x=0.8\pm0.1$ in $Ti_3Ge_xC_2$.

The conclusion that our films are substoichiometric in Ge is further supported by the fact that the relative peak intensities of the *0002* and *0008* peaks differ strongly from the ideal peak-intensity ratio of the stoichiometric compound, for which the 0008/0002 peak-intensity ratio is ~3 compared to ~28 for the present films. Simulations using the Carine and PowderCell softwares (not shown) show that this intensity difference is consistent with a Ge substoichiometry corresponding to an approximate composition of $Ti_3Ge_{0.8}C_2$. Although MAX-phases are described as

having 211, 312, or 413 stoichiometry, there exist stoichiometry ranges for vacancies at A and X sites, examples of this are $Ti_3AlC_{1.8}$ [4] and Ti_2AlC, where first-principles calculations have shown it to be stable for compositions as low as $Ti_2Al_{0.5}C$ [30]. Few investigations on the substoichiometry of MAX-phases synthesized in bulk form have been reported. A recent publication is the work of Cabioc´h et al. where the substoichiometry and solid solution effects in $Ti_2Al(C_x,N_{1-x})_y$ compounds was investigated. In this study it was found that significant deviations from the ideal composition of MAX-phases are possible to achieve [31]. It is likely that the observed substochiometry of Ti_3GeC_2 thin films could also be achieved in bulk Ti_3GeC_2. However, this has not been studied.

Figure 4 shows SEM images of a typical Ti_3GeC_2 film. The films have a step-flow growth pattern with {11 0} step facets, where the off-cut SiC surface provides the growth steps. The topography of the Ti_3GeC_2 films was also investigated using helium ion microscopy (HIM), which has a smaller probe size and a smaller interaction volume as compared to SEM, making it possible to achieve higher surface sensitivity and image resolution [32, 33]. Figure 5 displays a HIM image of one of the steps. The image confirms the hexagonal shape of the surface layers and reveals that what appears to be single terraces in the SEM (c.f. Figure 4) actually consists of several layers with thickness of a single crystal unit cell or fraction thereof.

AFM imaging in Figure 6 of the Ti_3GeC_2 film was used to quantify the heights of the terraces. The step heights were found to be half a unit cell, one unit cell, or multiples thereof, like with AFM observations made on Ti_3SiC_2 grown on SiC(0001) substrates [12]. For the case of Ti_3GeC_2, Figure 6 shows the presence of ~20 nm large particles on the surface of the film. This was also observed during HIM

imaging, and can be attributed to the segregation of Ge to the surface of the films. Surface segregation into Ge particles, several hundred nanometers in size, has been reported for Ti_2GeC_2 [15] and Cr_2GeC magnetron-sputtered thin films, and has been attributed to fast Ge-diffusion rates along the basal planes [19]. The out-diffusion of group-14 A elements in Ti-A-C MAX phases has been studied by Emmerlich et al., where no surface segregation was found for Ti_3SiC_2, while Ti_2GeC and Ti_2SnC had extensive surface segregations [15]. Since our films are substoichiometric in Ge, the supersaturation conditions required for formation of large islands are most likely not fulfilled. Therefore, small Ge particles (on the order of 20 nm), evenly distributed on the terraces, are formed rather than the larger Ge islands seen in Refs. [15] and [19].

The growth mode of the Ti_3GeC_2 films is similar to the step-flow growth that we have recently reported for the epitaxial growth of Ti_3SiC_2 films on 4H-SiC(0001) [12]. An interesting difference is that for the Ti_3SiC_2 films, Si-supersaturation growth conditions were necessary to maintain equilibrium-shape, hexagonal steps. The Ti_3GeC_2 films, however, grow with hexagonal steps for depositions made with the same growth conditions, which for Ti_3SiC_2 lead to {1 0 0} terrace edge truncation. The observations of equilibrium shape steps and the formation of Ge particles indicate that Ti_3GeC_2 is at equilibrium at a substoichiometric composition unlike Ti_3SiC_2, which requires supersaturation for nucleation and growth.

In order to study the possible application of the epitaxially grown Ti_3GeC_2 films as ohmic contacts to 4H-SiC, current-voltage (I-V) measurements were performed on TLM contact pads. The definition of an ohmic contact is that its current-voltage (I-V) curve is linear and symmetric. Figure 7 shows I-V curves measured on two neighboring contact pads with a 5 μm separation. As can be seen

from the I-V curves the Ti_3GeC_2 displays an almost ohmic behavior. Applying a high-temperature rapid thermal anneal might help achieve low-resistivity ohmic contacts to SiC, as seen for epitaxial Ti_3SiC_2 films after high temperature annealing at 950 ºC [11].

4 Conclusions

We have grown epitaxial Ti_3GeC_2 thin films with substoichiometry in Ge on 4° off-cut 4H-SiC(0001) substrates using DC magnetron sputtering from three separate targets. The growth mode of the Ti_3GeC_2 layers is lateral step-flow on (0001) terraces and with {11 0} step faceting. This differs from Ti_3SiC_2 where Si-*super*saturation conditions were necessary to achieve the hexagonal growth pattern. Finally, Ti_3GeC_2 films display an almost ohmic behavior with only self-annealing from the growth at 800 ºC.

Acknowledgements

Funding from the VINN Excellence Center in Research and Innovation on Functional Nanoscale Materials (FunMat) by the Swedish Governmental Agency for Innovation Systems (VINNOVA) is acknowledged. We thank the staff at the Tandem Laboratory, Uppsala University for support during the ERD analysis.

References

[1] M.W. Barsoum, T. El-Raghy, J. Amer. Cer. Soc. 79 (1996) 1953.

[2] M.W. Barsoum, D. Brodkin, T. El-Raghy, Scr. Mater. 36 (1997) 535.

[3] M.W. Barsoum, Prog. Solid State Chem. 28 (2000) 201.

[4] P. Eklund, M. Beckers, U. Jansson, H. Högberg, L. Hultman, Thin Solid Films 518 (2010) 1851.

[5] Z.M. Sun, Int. Mater. Rev. 56 (2011) 143.

[6] F. Goesmann, R. Schmid-Fetzer, Semicond. Sci. Technol. 10 (1995) 1652.

[7] Z. Wang, S. Tsukimoto, M. Saito, K. Ito, M. Murakami, Y. Ikuhara, Phys. Rev. B: Condens. Matter. 80 (2009) 245303.

[8] S. Tsukimoto, K. Ito, Z. Wang, M. Saito, Y. Ikuhara, M. Murakami, Mater. Trans. 50 (2009) 1071.

[9] B. Pécz, L. Tóth, M.A. di Forte-Poisson, J. Vacas, Appl. Surf. Sci. 206 (2003) 8.

[10] F. La Via, F. Roccaforte, A. Makhtari, V. Raineri, P. Musumeci, L. Calcagno, Microelectron. Eng. 60 (2002) 269.

[11] K. Buchholt, R. Ghandi, M. Domeij, C.-M Zetterling, J. Lu, P. Eklund, L. Hultman, A. Lloyd Spetz, Appl. Phys. Lett. 98 (2011) 042108.

[12] K. Buchholt, P. Eklund, J. Jensen, J. Lu, A. Lloyd Spetz, L. Hultman, Scr. Mater. 64 (2011) 1141.

[13] H. Högberg, P. Eklund, J. Emmerlich, J. Birch, L. Hultman, J. Mater. Res. 20 (2005) 779.

[14] T.H. Scabarozi, P. Eklund, J. Emmerlich, H. Högberg, T. Meehan, P. Finkel, M.W. Barsoum, J.D. Hettinger, L. Hultman, S.E. Lofland, Solid State Commun. 146 (2008) 498.

[15] J. Emmerlich, P. Eklund, D. Rittrich, H. Högberg, L. Hultman, J. Mater. Res. 22 (2007) 2279.

[16] T. El-Raghy, S. Chakraborty, M.W. Barsoum, J. Eur. Ceram. Soc. 20 (2000) 2619.

[17] S.E. Lofland, J.D. Hettinger, K. Harrell, P.Finkel, S. Gupta, M.W. Barsoum, G. Hug, Appl. Phys. Lett. 84 (2004) 508.

[18] O. Wilhelmsson, P. Eklund, H. Högberg, L. Hultman, U. Jansson, Acta Mater. 56 (2008) 2563.

[19] P. Eklund, M. Bugnet, V. Mauchamp, S. Dubois, C. Tromas, J. Jensen, L. Piraux, L. Gence, M. Jaouen, T. Cabioc'h, Phys. Rev. B 84 (2011) 075424.

[20] S. Kerdsongpanya, K. Buchholt, O. Tengstrand, J. Lu, J. Jensen, L. Hultman, P. Eklund, J. Appl. Phys. 110 (2011) 053516.

[21] T.H. Scabarozi, S. Benjamin, B. Adamson, J. Applegate, J. Roche, E. Pfeiffer, C. Steinmetz, C. Lunk, M.W. Barsoum, J.D. Hettinger, S.E. Lofland, Scr. Mater. 66 (2012) 85.

[22] N.J. Lane, S.C. Vogel, M.W. Barsoum, Phys. Rev. B 82 (2010) 174109.

[23] SiCrystal AG, Guenther-Scharowsky-Str.1, D91058 Erlangen, Germany.

[24] Acreo AB, Electrum 239, 164 40 Kista, Sweden.

[25] J. Emmerlich, H. Högberg, S. Sasvári, P. O. Å. Persson, L. Hultman, J. P. Palmquist, U. Jansson, J.M. Molina-Aldareguia, Z. Czigány, J. Appl. Phys. 96 (2004) 4817.

[26] H. J. Whitlow, G. Possnert, C.S. Petersson, Nucl. Instrum. Methods B. 27 (1987) 448.

[27] J. Jensen, D. Martin, A. Surpi, T. Kubart, Nucl. Instrum. Methods B. 268 (2010) 1893.

[28] M.S. Janson, CONTES Instruction Manual, Internal Report, Uppsala University, 2004.

[29] H. Högberg, L. Hultman, J. Emmerlich, T. Joelsson, P. Eklund, J.M. Molina-Aldareguia, J.-P. Palmquist, O. Wilhelmsson, U. Jansson, Surf. Coat. Technol. 193 (2005) 6.

[30] J. Wang, Y. Zhou, T. Liao, J. Zhang, Z. Lin, Scr. Mater. 58 (2008) 227.

[31] T. Cabioc´h, P. Eklund, V. Mauchamp, M. Jaouen, Accepted for publication in Journal of the European Ceramic Society.

[32] D. Cohen-Tanugi, N. Yao, J. Appl. Phys. 104 (2008) 063504.

[33] B.W. Ward, J.A. Notte, N.P. Economou, J. Vac. Sci. Technol. B 24 (2006) 2871.

FIGURE CAPTIONS

Figure 1 XRD pattern from a Ti_3GeC_2 film.

Figure 2 TEM image of a Ti_3GeC_2 film at (a) low, and (b) high magnification.

Figure 3 ToF-ERDA depth profile of a Ti_3GeC_2 film.

Figure 4 SEM image of a Ti_3GeC_2 film. Arrows indicate the SiC substrate crystal directions. Ti_3GeC_2 {11 0} step facets are also indicated.

Figure 5 HIM image of a Ti_3GeC_2 film.

Figure 6 AFM surface plot of a Ti_3GeC_2 film.

Figure 7 I-V curve from two neighboring Ti_3GeC_2 film contact pads on n- type 4H-SiC.

Highlights

Epitaxial growth of Ti_3GeC_2(0001) on 4H-SiC(0001) using magnetron sputtering.
Ti_3GeC_2 films grow by lateral step-flow with {11 0} faceting on the SiC surface.
Films are substoichiometric in Ge with small Ge particles present at the surface.

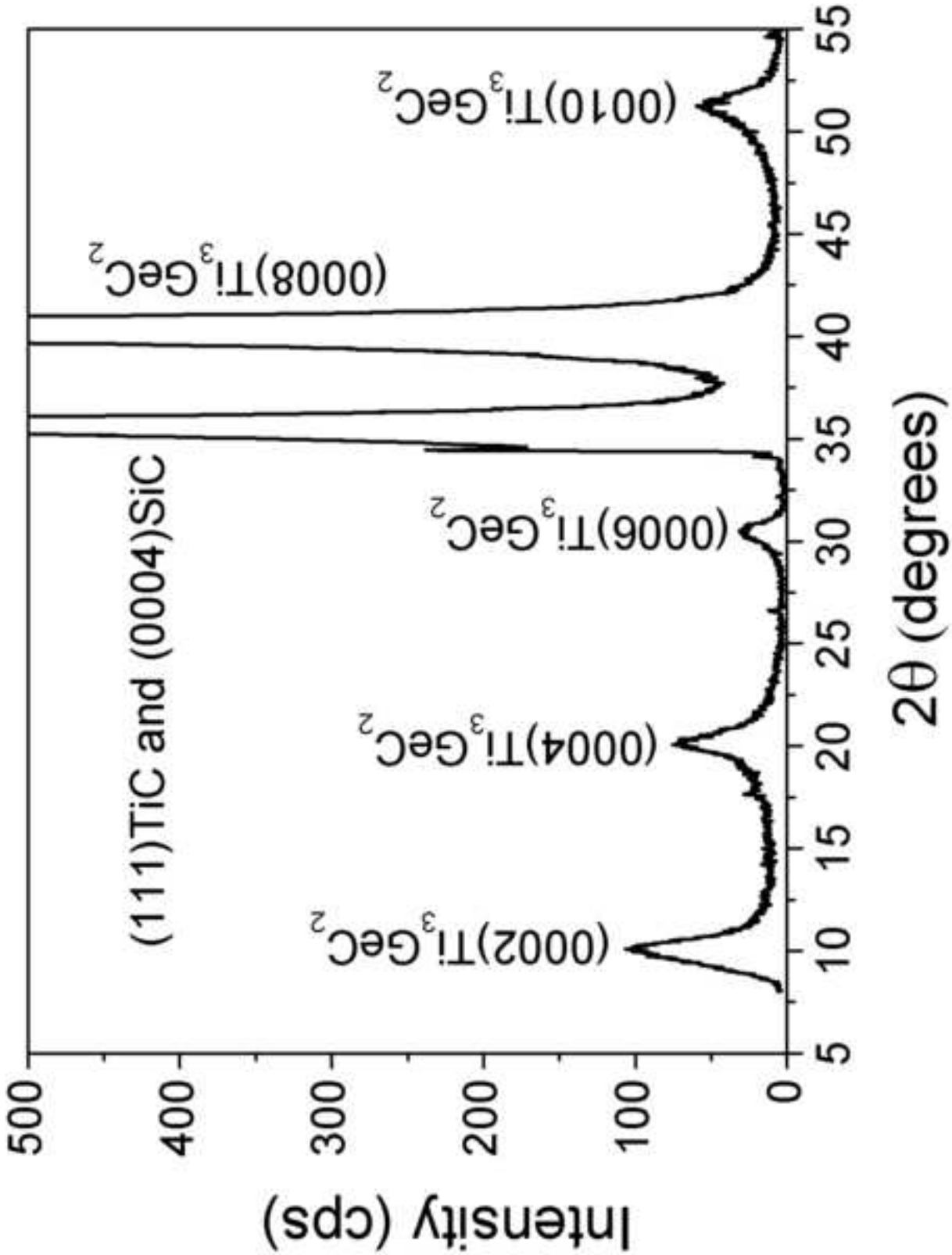
Intensity (cps)
2θ (degrees)
(0002)Ti3GeC2
(0004)Ti3GeC2
(0006)Ti3GeC2
(0008)Ti3GeC2
(0010)Ti3GeC2
(111)TiC and (0004)SiC
0
100
200
300
400
500
5
10
15
20
25
30
35
40
45
50
55

Figure(1)

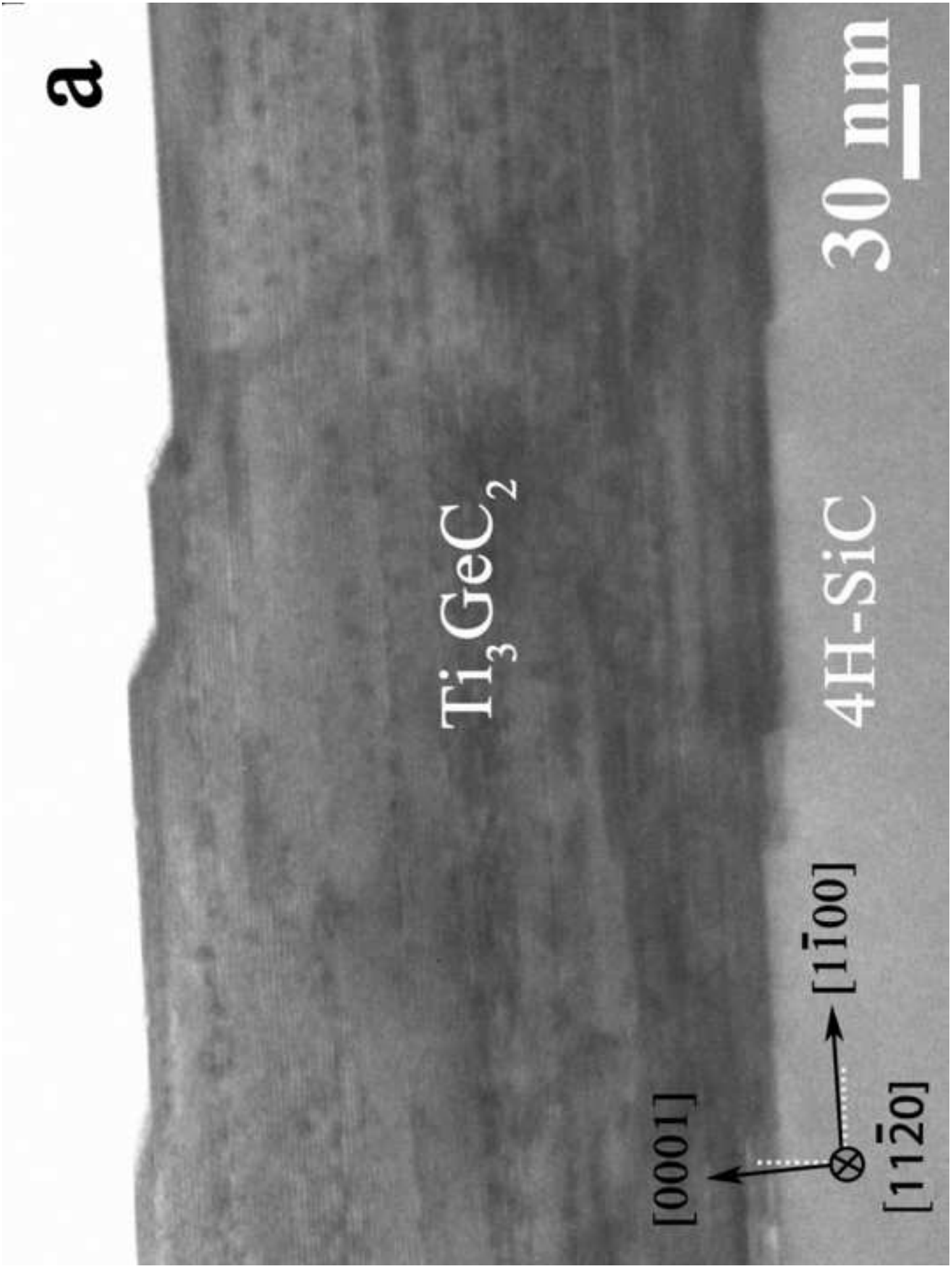

Figure(2a)

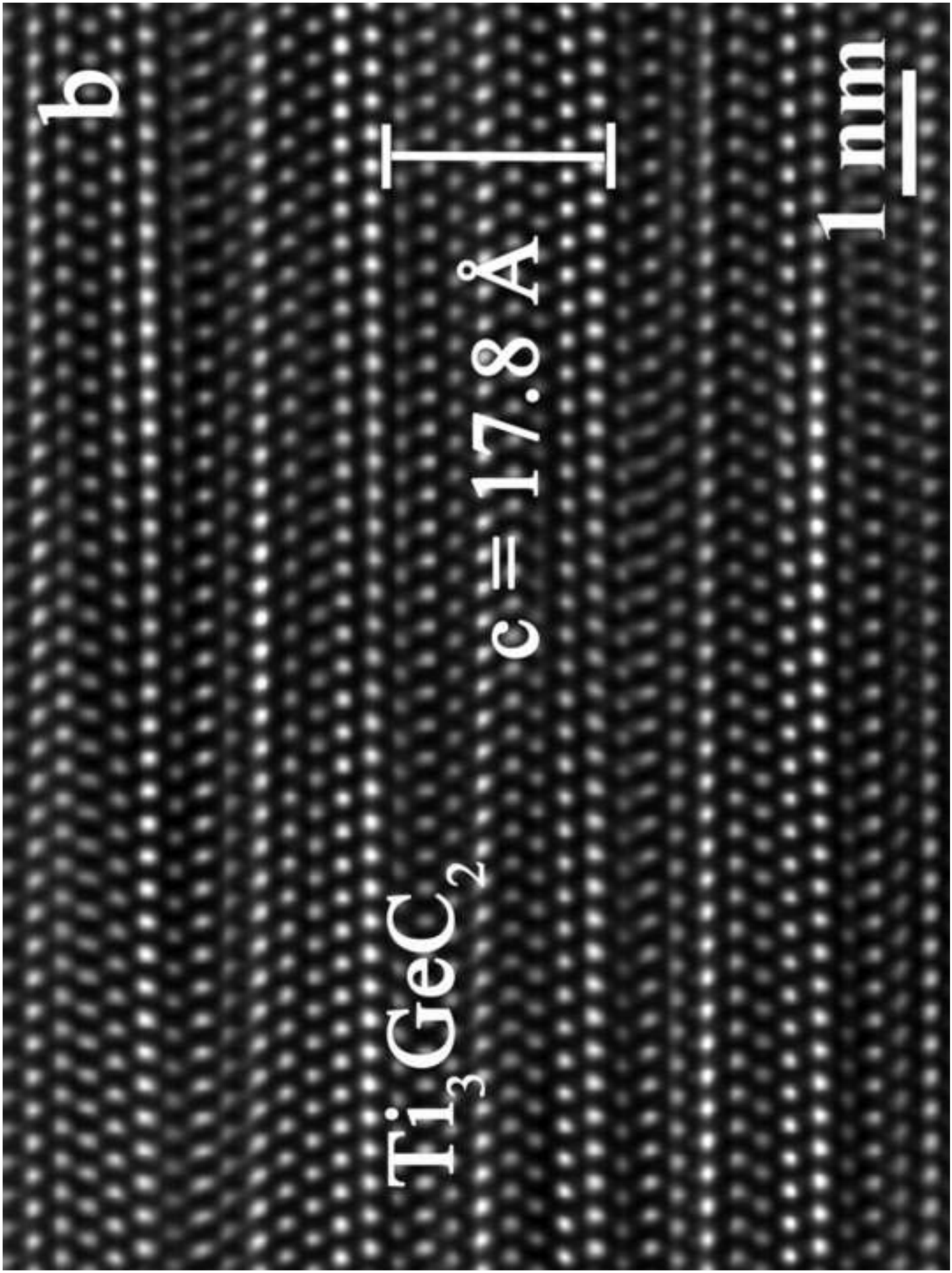

Figure(2b)

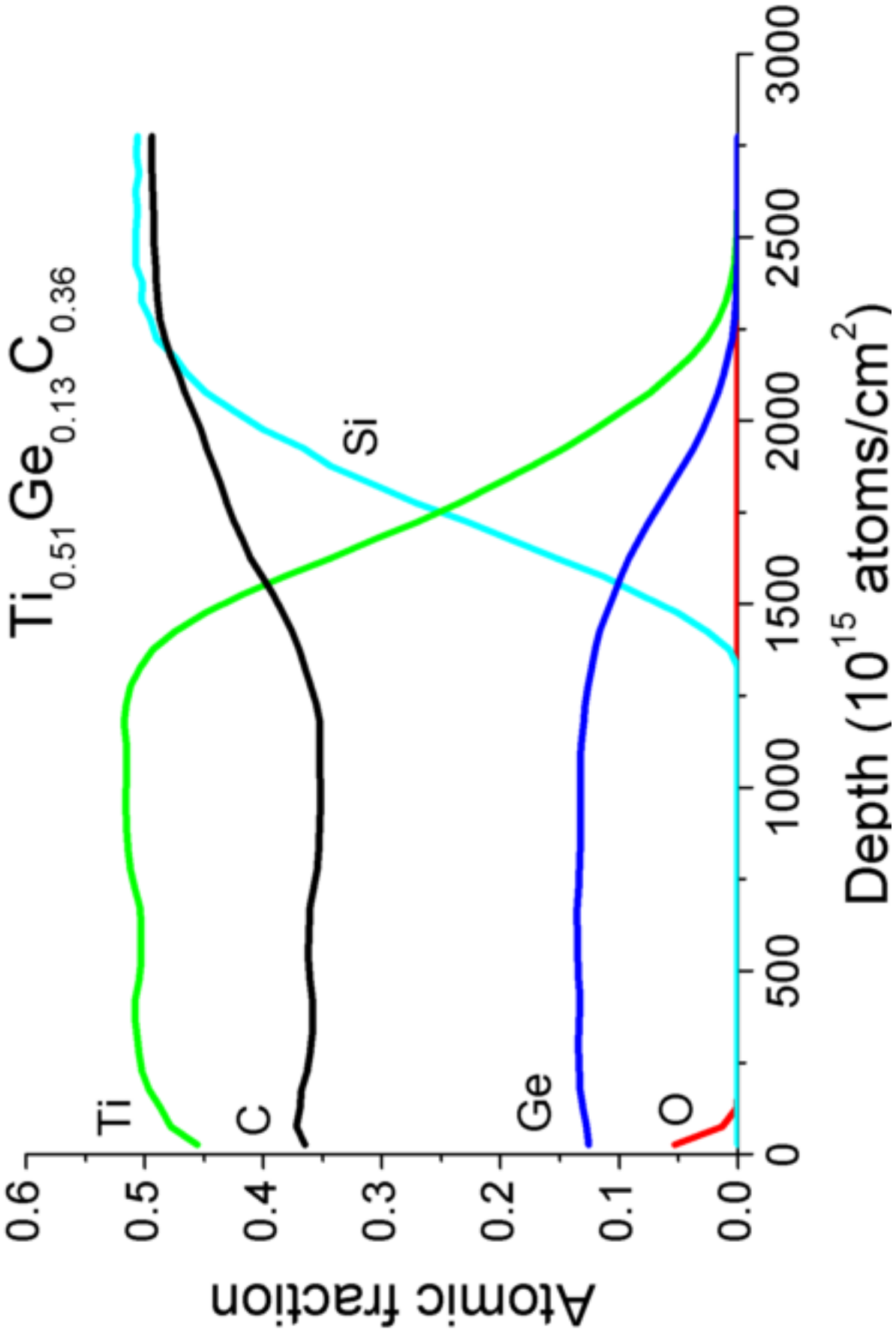
Ti0.51Ge0.13C0.36
Ti
C
Si
Ge
O
Atomic fraction
0.0
0.1
0.2
0.3
0.4
0.5
0.6
0
500
1000
1500
2000
2500
3000
Depth (10^15 atoms/cm^2)

Figure(3)

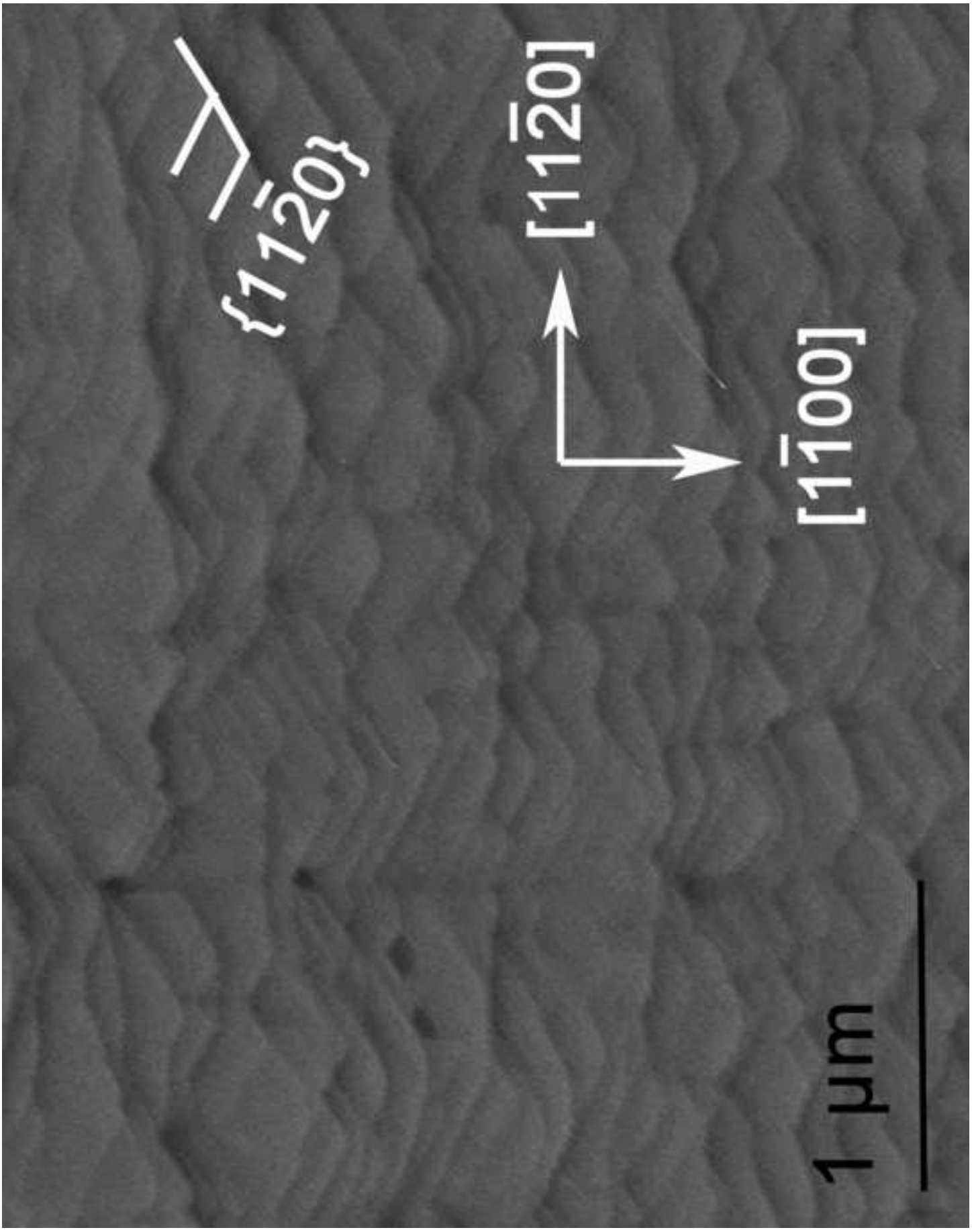

Figure(4)

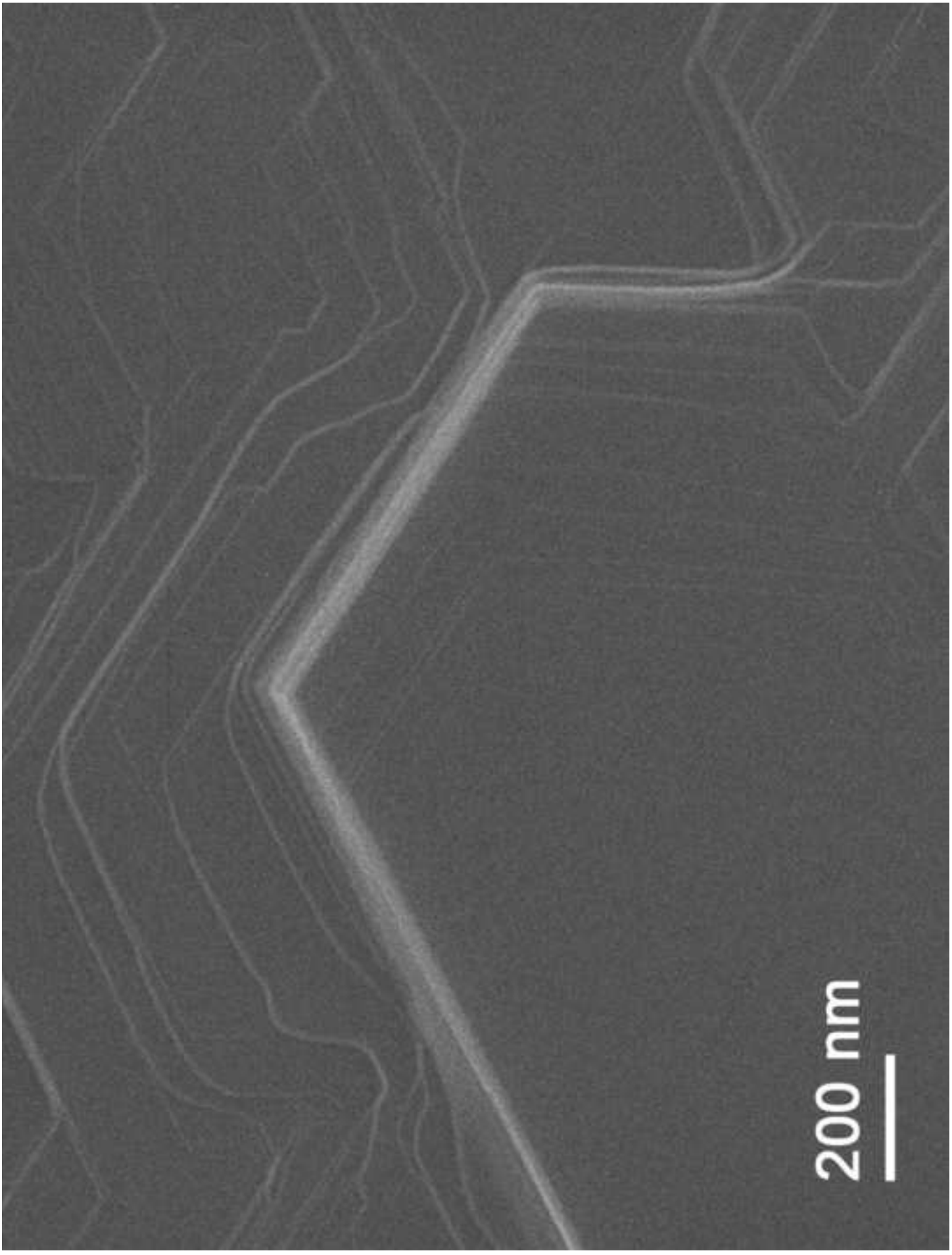

Figure(5)

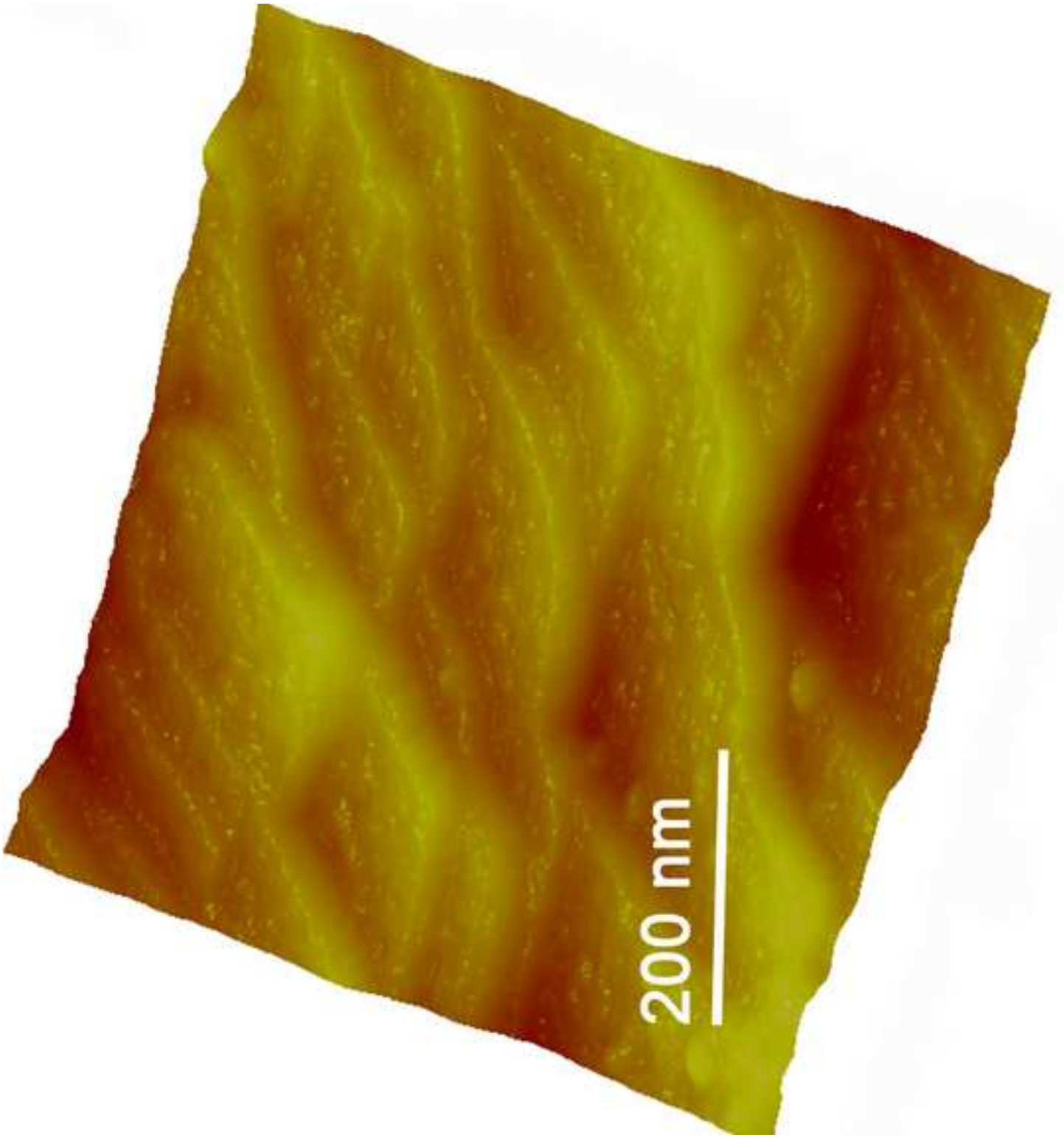

Figure(6)

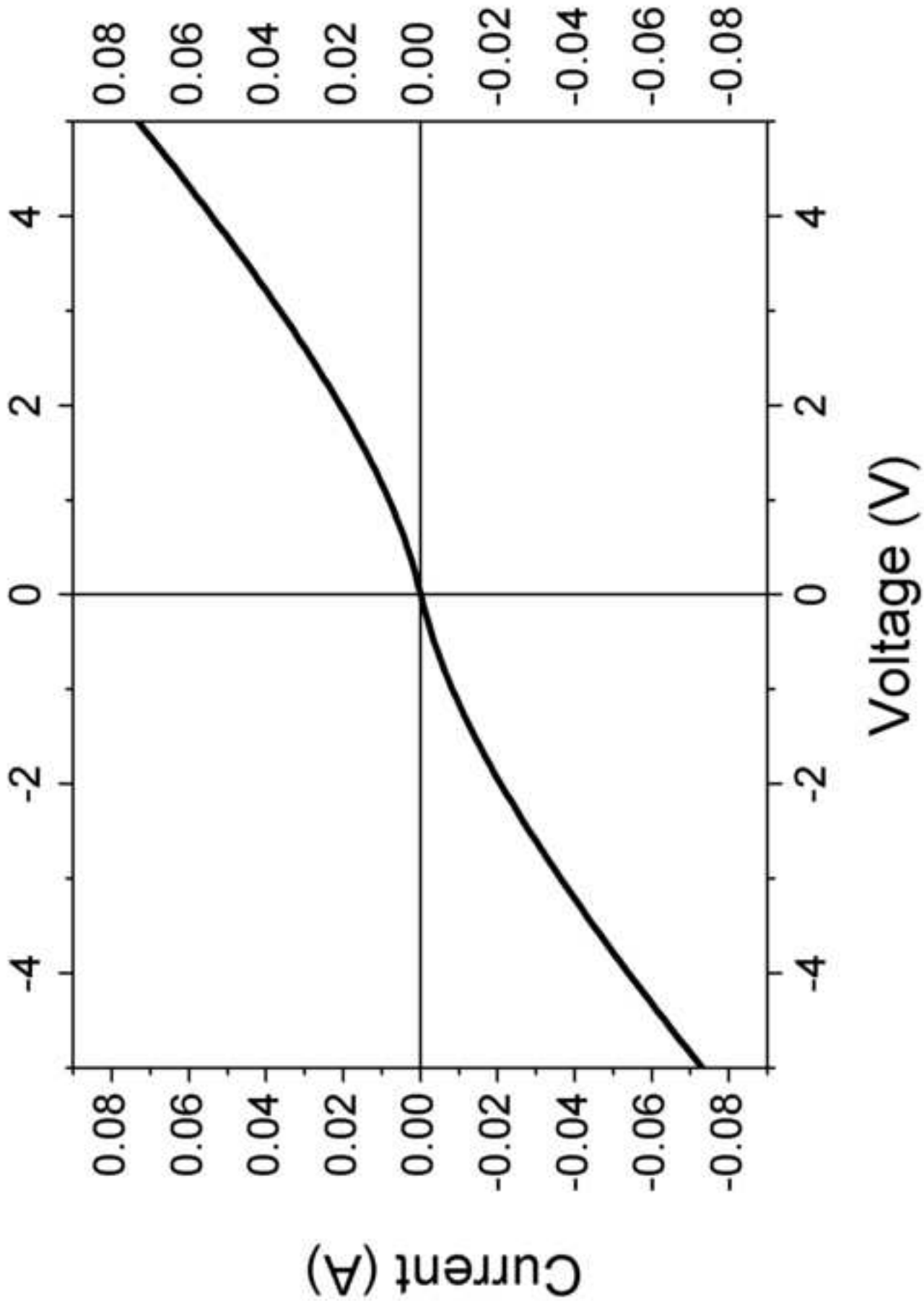

Figure(7)